Evaluating causal relations in neural systems: Granger causality, directed transfer function and statistical assessment of significance

Maciej Kamiński[1,2], **Mingzhou Ding**[1], **Wilson A. Truccolo**[1], **Steven L. Bressler**[1]

[1] Center for Complex Systems and Brain Sciences, Florida Atlantic University, 777 Glades Rd., Boca Raton, FL 33431, USA
[2] Laboratory of Medical Physics, Warsaw University, ul. Hoża 69, 00-681 Warsaw, Poland

Abstract. We consider the question of evaluating causal relations among neurobiological signals. In particular, we study the relation between the directed transfer function (DTF) and the well-accepted Granger causality, and show that DTF can be interpreted within the framework of Granger causality. In addition, we propose a method to assess the significance of causality measures. Finally, we demonstrate the applications of these measures to simulated data and actual neurobiological recordings.

1 Introduction

In neurobiology, as in many other fields of science and engineering, a question of great interest is whether there exist causal relations among a set of measured variables. First attempts at answering this question, which later evolved into the field of structural equation modeling (Asher 1983), can be found in the social sciences literature dating back to the 1950s. Based on the theory of independently realized multivariate random variables (i.e., not considering temporal information), structural equation modeling theoretically hypothesizes the direction of interaction among the variables and then quantifies the interaction strength with correlation analysis. The dependence on a theoretical framework makes the approach difficult to apply in cases where a theoretical framework is not well established or is absent.

Wiener (1956) recognized the importance of temporal ordering in the inference of causal relations from a pure statistical point of view and proposed that, for two simultaneously measured time series, one series can be called causal to the other if we can better predict the second time series by incorporating knowledge of the first one. This concept was later adopted and formalized by Granger (1969) in the context of linear regression models of stochastic processes. Specifically, if the variance of the prediction error for the second time series at the present time is reduced by including past measurements from the first time series in the linear regression model, then the first time series can be said to cause the second time series. Granger's concept of causality has received a great deal of attention and has been applied widely in the econometrics literature. Geweke's novel decomposition of the multivariate autoregressive process (Geweke 1982) led to a set of causality measures which have a spectral representation and make the interpretation more straightforward.

In the 1970s and 1980s engineers extended Granger's ideas to linear systems theory. Caines and Chan (1975) and Gevers and Anderson (1981) introduced the concept of causality to the study of feedback relations between input and output variables. Their measures are all conveniently expressed in the spectral domain and have been subsequently adopted by researchers in other fields.

Applications of causal measures in neurobiology started in the early 1980s. Saito and Harashima (1981) introduced the method of directed coherence to study the relation between a pair of data channels described by a bivariate autoregressive process. This method has been applied to clinical problems (Saito and Harashima 1981) and to the investigation of interdependence between the two cerebral hemispheres (Wang and Takigawa 1992). Schnider et al. (1989) used results given by Gevers and Anderson (1981) to detect feedback interactions between parkinsonian tremor and cell activities in the thalamus. More recently, Bernasconi and Konig (1999) applied Geweke's spectral measures to detect causal influences among different areas in the cat visual cortex. Sameshima and Baccalá (1999) developed a partial causality measure and applied it to spike train data analysis. A similar measure was proposed by Schack et al. (1995).

It should be noted that most of the methods mentioned above deal with bivariate time series, or two non-overlapping sets of time series, and do not make use of the whole covariance structure for multichannel data. Such pairwise treatment, as we will show in this work,

Correspondence to: M. Ding
(e-mail: ding@fau.edu)

can lead to erroneous results that otherwise could be avoided in a full multivariate approach. Kamiński and Blinowska (1991) proposed a full multivariate spectral measure, called the directed transfer function (DTF), which is used to determine the directional influences between any given pair of channels in a multivariate data set. The DTF has the advantage of requiring that only one multivariate autoregressive (MVAR) model be estimated from recordings of all the channels. This method has been applied to a number of neurobiological systems and is the main focus of this work. Since the DTF function is motivated from the perspective of spectral domain transfer functions, its relation to Granger causality, which is most clearly defined in terms of linear regression coefficients in the time domain, remains unclear, thereby hampering interpretation of the DTF function.

The main contributions of this work are as follows:

1. We perform a detailed analysis of the DTF function and show that it can be interpreted in terms of Granger causality. This allows us to utilize the convenience and full multivariate power of the DTF function, while maintaining the well-accepted interpretation of Granger causality.

2. We show that a nonzero value of DTF or Granger causality does not necessarily imply that the causal influence between the two evaluated channels is direct. It is possible that the effect is mediated by another channel or by another group of channels, or by variables that are not included in the measurements. We propose a measure, referred to henceforth as direct causality (DC), which can be used to give further information about whether a direct link exists between two given channels.

3. All of the causality measures that we consider are highly nonlinear functions of the data and, consequently, the distributions of their estimators are often unknown. This problem hinders one's ability to assess the statistical significance of the estimates. We propose a possible solution to this problem by using a surrogate data technique. Specifically, with this technique one generates an empirical distribution for a given estimator in which interactions between channels are removed. Significance tests can then be performed based on this empirical distribution.

4. The DTF function is a highly complex statistical variable. To gain confidence in its usefulness for data analysis, we study its behavior when applied to simulated field potential time series generated by neural models having built-in causality patterns. We also discuss the important complementary role of DC in the same model simulations.

5. Using data generated by models of spiking neurons, we show that the DTF function can also measure causal relations among interacting point processes. This extends the applicability of this measure to single-unit studies.

6. We demonstrate the utility of the proposed causality measures in two neurobiological examples. One of them deals with human sleep data and the other concerns a visual pattern discrimination task in the monkey. In the context of the second example, we stress the importance of combining the causality measures with a recently proposed short window spectral analysis technique for cognitive experiments (Ding et al. 2000) to capture the rapidly changing cognitive state of the brain.

2 Theoretical considerations

2.1 Granger causality

Let $X_1(t)$ and $X_2(t)$ denote the time series from two data channels. (The same discussion applies to the case where $\mathbf{X}_1(t)$ and $\mathbf{X}_2(t)$ are vectors, representing two sets of nonoverlapping channels.) Suppose that the temporal dynamics of $X_1(t)$ and $X_2(t)$ are suitably represented by the following bivariate autoregressive process:

$$X_1(t) = \sum_{j=1}^{p} A_{11}(j)X_1(t-j) + \sum_{j=1}^{p} A_{12}(j)X_2(t-j) + E_1(t)$$

$$X_2(t) = \sum_{j=1}^{p} A_{21}(j)X_1(t-j) + \sum_{j=1}^{p} A_{22}(j)X_2(t-j) + E_2(t) \; .$$

$$(1)$$

If the variance of the prediction error E_1 (or E_2) is reduced by the inclusion of the X_2 (or X_1) terms in the first (or second) equation, then, based on Granger causality, we say that X_2 (or X_1) causes X_1 (or X_2). An equivalent but more convenient way of expressing the same concept is that coefficients $A_{12}(j)$ (or $A_{21}(j)$), $j = 1, 2, \ldots, p$, are not uniformly zero under suitable statistical criteria.

To examine the causal relations in the spectral domain, we Fourier transform (1) to obtain

$$\begin{pmatrix} A_{11}(f) & A_{12}(f) \\ A_{21}(f) & A_{22}(f) \end{pmatrix} \begin{pmatrix} X_1(f) \\ X_2(f) \end{pmatrix} = \begin{pmatrix} E_1(f) \\ E_2(f) \end{pmatrix} \qquad (2)$$

where the components of the $\mathbf{A}(f)$ matrix are

$$A_{lm}(f) = \delta_{lm} - \sum_{j=1}^{p} A_{lm}(j)e^{-i2\pi f j}$$

$$\delta_{lm} = \begin{cases} 1 & \text{when } l = m \\ 0 & \text{when } l \neq m \; . \end{cases}$$

$$(3)$$

Rewriting (2) as

$$\begin{pmatrix} X_1(f) \\ X_2(f) \end{pmatrix} = \begin{pmatrix} H_{11}(f) & H_{12}(f) \\ H_{21}(f) & H_{22}(f) \end{pmatrix} \begin{pmatrix} E_1(f) \\ E_2(f) \end{pmatrix} \qquad (4)$$

we have

$$\begin{pmatrix} H_{11}(f) & H_{12}(f) \\ H_{21}(f) & H_{22}(f) \end{pmatrix} = \begin{pmatrix} A_{11}(f) & A_{12}(f) \\ A_{21}(f) & A_{22}(f) \end{pmatrix}^{-1} \qquad (5)$$

as the transfer matrix. Using the definition of matrix inversion, the Granger causality from channel j to channel i in the spectral domain can be defined in terms of the off-diagonal elements of the transfer matrix (Caines and Chan 1975). Namely

$$I_{j \to i}^2 = |H_{ij}(f)|^2 = \frac{|A_{ij}(f)|^2}{|\mathbf{A}(f)|^2} \quad . \tag{6}$$

2.2 Directed transfer function

In the above definition of Granger causality only two channels (or two sets of channels) are considered. Now we describe a multivariate method that gives pairwise directional information from one autoregressive model fit to a larger number of channels. Specifically, let $\mathbf{X}(t) = [X_1(t), X_2(t), \ldots, X_k(t)]^{\mathrm{T}}$ denote the measurement from k channels at time t. Here T denotes matrix transposition. Suppose that $\mathbf{X}(t)$ is adequately described by the following MVAR process:

$$\mathbf{X}(t) = \sum_{i=1}^{p} \mathbf{A}(i)\mathbf{X}(t-i) + \mathbf{E}(t) \tag{7}$$

Transforming this equation to the frequency domain yields

$$\mathbf{A}(f)\mathbf{X}(f) = \mathbf{E}(f) \tag{8}$$

where

$$\mathbf{A}(f) = -\sum_{j=0}^{p} \mathbf{A}(j)\mathrm{e}^{-i2\pi f j}$$

with $\mathbf{A}(0) = -\mathbf{I}$ ($\mathbf{I}$ being the identity matrix). Equation (8) can be rewritten as:

$$\mathbf{X}(f) = \mathbf{A}^{-1}(f)\mathbf{E}(f) = \mathbf{H}(f)\mathbf{E}(f) \tag{9}$$

Here $\mathbf{H}$ is the transfer matrix of the system. Patterned on the two-channel Granger causality measure in the frequency domain, (6), the DTF from channel j to channel i, representing the causal influence from j to i, is defined as

$$\theta_{ij}^2(f) = |H_{ij}(f)|^2 \quad . \tag{10}$$

The normalized DTF is defined as (Kamiński and Blinowska 1991):

$$\gamma_{ij}^2(f) = \frac{|H_{ij}(f)|^2}{\sum_{m=1}^{k} |H_{im}(f)|^2} \quad , \tag{11}$$

which expresses the ratio of influence of channel j to channel i to the joint influences from all the other channels to the channel i, and has a value between 0 and 1.

2.3 Granger causality and DTF

For a bivariate process, the non-normalized DTF function, (10), is equivalent to the spectral Granger causality, (6), which is directly related to the MVAR coefficients. But, for the multivariate case, the relation between the off-diagonal entries in the transfer matrix $\mathbf{H}(f)$, which are the basis of the DTF function, and the MVAR coefficients remains unclear. Recognizing that a bivariate autoregressive model can always be extracted by variable elimination from the full multivariate model containing the two channels, we now show that – through matrix analysis – one can establish the relation between the off-diagonal elements of $\mathbf{H}(f)$ and the appropriate MVAR coefficients, making it possible to interpret the multivariate DTF function within the framework of Granger causality.

Without loss of generality, consider the first two channels in the MVAR model, (8). Partition the matrix $\mathbf{A}(f)$ into the following block form

$$\begin{pmatrix} \begin{pmatrix} A_{11} & A_{12} \\ A_{21} & A_{22} \end{pmatrix} & \begin{pmatrix} A_{13} & \cdots & A_{1p} \\ A_{23} & \cdots & A_{2p} \end{pmatrix} \\ \begin{pmatrix} A_{31} & A_{32} \\ \vdots & \vdots \\ A_{p1} & A_{p2} \end{pmatrix} & \begin{pmatrix} A_{33} & \cdots & A_{3p} \\ \vdots & \ddots & \vdots \\ A_{p3} & \cdots & A_{pp} \end{pmatrix} \end{pmatrix} \begin{pmatrix} \begin{pmatrix} X_1 \\ X_2 \end{pmatrix} \\ \begin{pmatrix} X_3 \\ \vdots \\ X_p \end{pmatrix} \end{pmatrix}$$

$$= \begin{pmatrix} \begin{pmatrix} E_1 \\ E_2 \end{pmatrix} \\ \begin{pmatrix} E_3 \\ \vdots \\ E_p \end{pmatrix} \end{pmatrix} \tag{12}$$

Introducing matrix block notation

$$\mathbf{A}(f) = \begin{pmatrix} \mathbf{A}_{11} & \mathbf{A}_{12} \\ \mathbf{A}_{21} & \mathbf{A}_{22} \end{pmatrix}$$

the above equation can be further written as:

$$\mathbf{A}_{11}\begin{pmatrix} X_1 \\ X_2 \end{pmatrix} + \mathbf{A}_{12}\begin{pmatrix} X_3 \\ \vdots \\ X_p \end{pmatrix} = \begin{pmatrix} E_1 \\ E_2 \end{pmatrix} \tag{13a}$$

$$\mathbf{A}_{21}\begin{pmatrix} X_1 \\ X_2 \end{pmatrix} + \mathbf{A}_{22}\begin{pmatrix} X_3 \\ \vdots \\ X_p \end{pmatrix} = \begin{pmatrix} E_3 \\ \vdots \\ E_p \end{pmatrix} \tag{13b}$$

From (13b) we obtain:

$$\begin{pmatrix} X_3 \\ \vdots \\ X_p \end{pmatrix} = -\mathbf{A}_{22}^{-1}\mathbf{A}_{21}\begin{pmatrix} X_1 \\ X_2 \end{pmatrix} + \mathbf{A}_{22}^{-1}\begin{pmatrix} E_3 \\ \vdots \\ E_p \end{pmatrix} \quad .$$

Using this result to eliminate variables in (13a) we have:

$$(\mathbf{A}_{11} - \mathbf{A}_{12}\mathbf{A}_{22}^{-1}\mathbf{A}_{21})\begin{pmatrix} X_1 \\ X_2 \end{pmatrix}$$

$$= \begin{pmatrix} E_1 \\ E_2 \end{pmatrix} - \mathbf{A}_{12}\mathbf{A}_{22}^{-1}\begin{pmatrix} E_3 \\ \vdots \\ E_p \end{pmatrix} = \begin{pmatrix} E_1' \\ E_2' \end{pmatrix} \quad . \tag{14}$$

This equation is the Fourier transform of a bivariate model involving only channels 1 and 2 with E_1' and E_2' being the Fourier transforms of the new noise sources. Knowing that

$$\left(\mathbf{A}_{11} - \mathbf{A}_{12}\mathbf{A}_{22}^{-1}\mathbf{A}_{21}\right) = \begin{pmatrix} A_{11} - (A_{13}\cdots A_{1p})\mathbf{A}_{22}^{-1}\begin{pmatrix} A_{31} \\ \vdots \\ A_{p1} \end{pmatrix} & A_{12} - (A_{13}\cdots A_{1p})\mathbf{A}_{22}^{-1}\begin{pmatrix} A_{32} \\ \vdots \\ A_{p2} \end{pmatrix} \\ A_{21} - (A_{23}\cdots A_{2p})\mathbf{A}_{22}^{-1}\begin{pmatrix} A_{31} \\ \vdots \\ A_{p1} \end{pmatrix} & A_{22} - (A_{23}\cdots A_{2p})\mathbf{A}_{22}^{-1}\begin{pmatrix} A_{32} \\ \vdots \\ A_{p2} \end{pmatrix} \end{pmatrix}$$

We can rewrite (14) as:

$$\begin{pmatrix} X_1 \\ X_2 \end{pmatrix} = \frac{1}{|\mathbf{A}_{11} - \mathbf{A}_{12}\mathbf{A}_{22}^{-1}\mathbf{A}_{21}|} \begin{pmatrix} \left|A_{22} - (A_{23}\cdots A_{2p})\mathbf{A}_{22}^{-1}\begin{pmatrix} A_{32} \\ \vdots \\ A_{p2} \end{pmatrix}\right| & -\left|A_{12} - (A_{13}\cdots A_{1p})\mathbf{A}_{22}^{-1}\begin{pmatrix} A_{32} \\ \vdots \\ A_{p2} \end{pmatrix}\right| \\ -\left|A_{21} - (A_{23}\cdots A_{2p})\mathbf{A}_{22}^{-1}\begin{pmatrix} A_{31} \\ \vdots \\ A_{p1} \end{pmatrix}\right| & \left|A_{11} - (A_{13}\cdots A_{1p})\mathbf{A}_{22}^{-1}\begin{pmatrix} A_{31} \\ \vdots \\ A_{p1} \end{pmatrix}\right| \end{pmatrix} \begin{pmatrix} E_1' \\ E_2' \end{pmatrix}.$$

Following (6), using entries from the transfer matrix, the causal influence from channel 1 to 2 can be defined as:

$$I_{1\to2}^2 = \frac{\left|A_{21} - (A_{23}\cdots A_{2p})\mathbf{A}_{22}^{-1}\begin{pmatrix} A_{31} \\ \vdots \\ A_{p1} \end{pmatrix}\right|^2}{|\mathbf{A}_{11} - \mathbf{A}_{12}\mathbf{A}_{22}^{-1}\mathbf{A}_{21}|^2}. \tag{15}$$

Recalling the following matrix algebra fact:

$$\begin{vmatrix} \mathbf{U} & \mathbf{V} \\ \mathbf{W} & \mathbf{D} \end{vmatrix} = |\mathbf{U} - \mathbf{V}\mathbf{D}^{-1}\mathbf{W}||\mathbf{D}|$$

we get the result:

$$I_{1\to2}^2 = \frac{\left|A_{21} - (A_{23}\cdots A_{2p})\mathbf{A}_{22}^{-1}\begin{pmatrix} A_{31} \\ \vdots \\ A_{p1} \end{pmatrix}\right|^2 |\mathbf{A}_{22}|^2}{|\mathbf{A}_{11} - \mathbf{A}_{12}\mathbf{A}_{22}^{-1}\mathbf{A}_{21}|^2 |\mathbf{A}_{22}|^2}$$

$$= \frac{|\mathbf{M}_{12}|^2}{|\mathbf{A}(f)|^2} \tag{16}$$

where $|\mathbf{M}_{ij}|$ is a minor of the matrix $\mathbf{A}$ with row i and column j removed.

Now we turn our attention to the DTF function. Refer to (9). The non-normalized DTF function is:

$$\theta_{21}^2(f) = |H_{21}(f)|^2 = \left|\left[\mathbf{A}^{-1}(f)\right]_{21}\right|^2 = \frac{|\mathbf{M}_{12}|^2}{|\mathbf{A}(f)|^2}$$

based on the definition of matrix inversion. This is the same expression as for Granger causality (15), thereby establishing that the DTF function can be interpreted in terms of Granger causality.

2.4 DC measure

It is important to realize that a nonzero value of the Granger causality measure does not necessarily mean that the two channels interact directly. A benefit of multivariate model fitting is that it uses information from all the channels, allowing us to ask whether there exists a direct causal influence between any two channels while the effects of all the other channels are taken into account. Specifically, referring to (7), if $A_{ij}(t), t = 1, 2, \ldots, p$, are not uniformly zero, we say that there is a direct causal influence from channel j to channel i, and define the DC measure:

$$D_{ij}^2 = \sum_{t=1}^{p} A_{ij}^2(t) \tag{17}$$

to evaluate the level of this influence. The same goal can be achieved using the Fourier transformed quantity $|A_{ij}(f)|^2$ (Sameshima and Baccalá 1999).

We note that, although the DTF function is computed from the full multivariate model, careful analysis of its definition indicates that it is in fact a linear combination of both the direct influence from one channel to another and the influence mediated by the other channels along various causal pathways. We illustrate this point by considering the DTF from channel 1 to channel 2 in a three-channel situation. From the definition of matrix inversion, the non-normalized DTF function follows from (10) as:

$$\theta_{21}^2(f) = |H_{21}(f)|^2 = \frac{|A_{21}(f)A_{33}(f) - A_{31}(f)A_{23}(f)|^2}{|\mathbf{A}(f)|^2} \tag{18}$$

Clearly, even if the direct influence from channel 1 to channel 2, $A_{21}(f)$, is zero, the above quantity may still be different from zero since there is an influence from 1 to 3 ($A_{31}(f)$) and from 3 to 2 ($A_{23}(f)$). The linkage from channel 1 to 3 to 2 will be a causal pathway if all the direct causal influences along the way are not zero.

Equation (18) raises another interesting question. Namely, even if $A_{21}(f)A_{33}(f)$ and $A_{31}(f)A_{23}(f)$ are both nonzero, their linear combination in the above expression still could be zero. Thus a zero DTF value may not mean a total absence of causal influence between the two channels. We give an explicit example of such a situation in Appendix A. Due to the possibility of this situation occurring, it is crucial to examine the DC measure to have a more precise understanding of the connection patterns.

2.5 Statistical test for significance

Both the DTF function and the DC measure have a highly nonlinear relation to the time series data from which they are derived. As a result, the distributions of their estimators are not well established. This makes tests of significance difficult to perform. Here we propose an empirical distribution technique using surrogate data (Theiler et al. 1992) to deal with this problem. Specifically, we randomly and independently shuffle the time series data from each channel to create a surrogate data set. Then a model is fitted to this surrogate data set and causal measures are derived from the model. Carrying out this process many times, each time performed on a new surrogate data set, we can create an empirical distribution for the causal measures. Since the construction is designed so that there is no interaction among the channels, these distributions give the estimator behavior for the null hypothesis case. Using this distribution we can then assess the significance of the causal measures evaluated from the actual data. The effectiveness of this technique will be examined in the next section on simulated examples.

3 Simulated examples

In this section we study the behavior of the DTF function and DC measure using simulated models with built-in causality patterns, and evaluate the effectiveness of the surrogate-data-based significance test. Two classes of model are considered: (1) a continuous neural population model mimicking local field potential (LFP) recordings, and (2) an integrate-and-fire-type point process model mimicking spike train data.

3.1 Two-channel LFP model

Interacting neural populations are modeled by coupled nonlinear ordinary differential equations. Mathematical details can be found in Appendix B. We fit a bivariate autoregressive model of order five to the simulated data, which comes in the form of a single long trial, normalized to have zero mean and unity variance. Equivalent results

can be obtained by fitting models to multiple trials of shorter segments of simulated data (Ding et al. 2000; Liang et al. 2000) (see the analysis of actual recordings in Sect. 4 for further elaboration on this point).

We consider two different coupling schemes. The first scheme is shown in Fig. 1a where there is a unidirectional coupling from channel 1 to channel 2. As expected, substantial causal influence exists from channel 1 to channel 2 for both the normalized DTF (Fig. 1b) and the non-normalized DTF (Fig. 1c), while the values of reverse influence are very small. To examine the statistical significance of these reverse influence values we adopt the surrogate data strategy discussed in the previous section. Specifically, we perform random and independent shuffling of the time series for each channel of the simulated data. A bivariate autoregressive model is fit to the shuffled data and the DTF functions are computed from the model. Carrying out the procedure for 100 such independently shuffled data sets we are able to construct an empirical distribution for the DTF functions. Since the shuffling procedure destroys all the
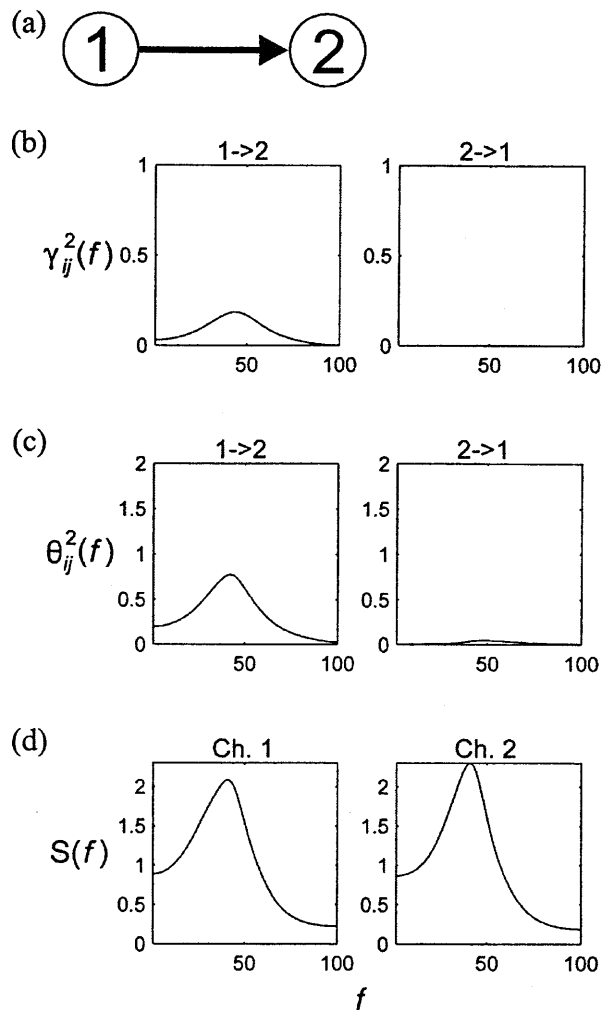

Fig. 1a–d. Results of a two-channel local field potential (LFP) model where the coupling is unidirectional: **a** coupling scheme; **b** normalized directed transfer function (DTF); **c** non-normalized DTF; **d** power spectra; **b–d** plotted as a function of frequency (Hz)
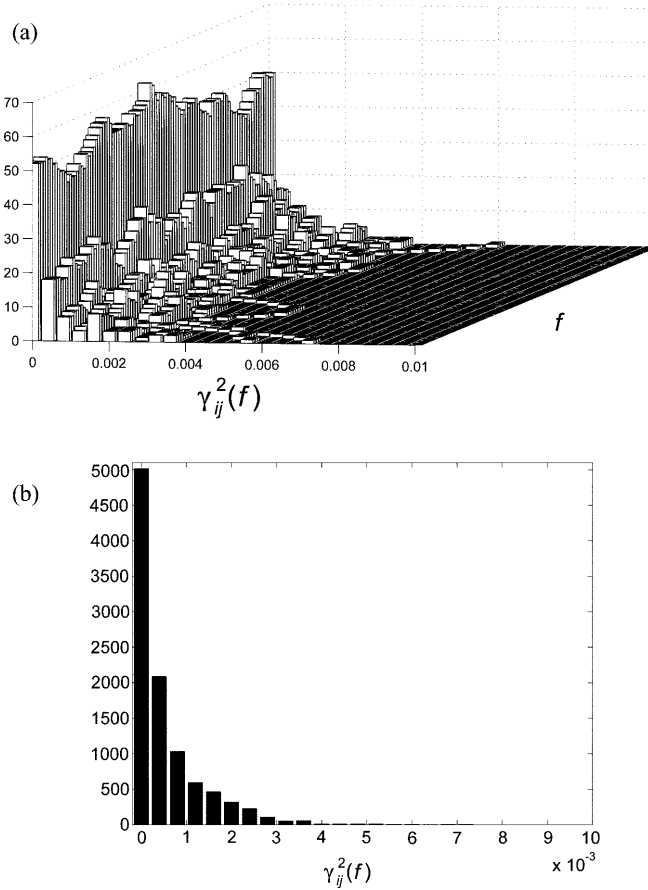
(a)

$\gamma_{ij}^2(f)$

(b)

$\gamma_{ij}^2(f)$

Fig. 2a,b. Distributions of DTF values resulting from 100 surrogate data sets. **a** Histograms for normalized θ_{21}^2 as a function of frequency; **b** histogram by combining results from all frequencies

(a)

(b)

Fig. 3a,b. Normalized **a** and non-normalized **b** DTF functions from channel 2 to channel 1 from Fig. 1 plotted together with the significance level obtained from Fig. 2, as functions of frequency (Hz)

temporal structure in the data, this empirical distribution gives the variability for the DTF functions when the null hypothesis of no causal influence is true.

Figure 2a shows the histogram of the surrogate normalized DTF function values as a function of frequency. Since the distribution is frequency independent by construction, we can combine the samples from all the frequencies into a single distribution (Fig. 2b). Without having an explicit formulation for the shape of this distribution, we compute an empirical threshold for a given significance level. The threshold value is further corrected for multiple comparisons by Dunn's method (Kirk 1995). Since the DTF is evaluated at 100 frequencies the Dunn-corrected threshold at $P < 0.05$ is 0.0045 for the normalized DTF and 0.068 for the non-normalized DTF.

Figure 3 shows both normalized and non-normalized DTF functions from channel 2 to channel 1, and the corresponding threshold values. As expected, both functions lie below their respective threshold, indicating the absence of causal influence from channel 2 to channel 1.

Another aspect we examine in Fig. 1 is frequency dependence of the DTF functions. Comparison of the DTF function spectra with the power spectra in Fig. 1d reveals very similar frequency profiles. This means that the DTF function shares the same frequency charac-
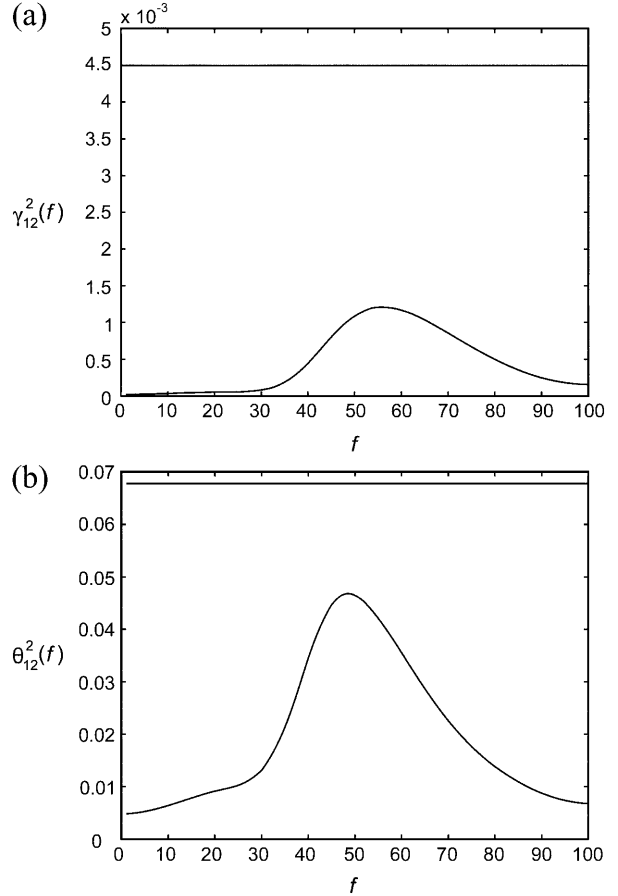
istics as the signals themselves. This property is observed both for simulated examples and for actual field-potential recordings, and makes the frequency dependence of the causal measures interpretable in terms of the overall frequency structure of the data. This effect can be understood from the fact that both the power spectra and the DTF functions are derived from the same transfer functions.

We next examine the meaning of the magnitudes of the DTF functions. In Fig. 4, normalized and non-normalized DTF values at the peak frequency are plotted against the connection strength between the two simulated neural populations. One can see that these functions rise monotonically with increasing connection strength. For the normalized DTF, Fig. 4b, saturation occurs as the connection strength increases, whereas the non-normalized DTF increases much more as a linear function of the connection strength.

The second coupling scheme is shown in Fig. 5a, where the interaction is reciprocal. As expected, the normalized (Fig. 5b) and non-normalized (Fig. 5c) DTF functions exhibit strong influences in both directions. Interestingly, the non-normalized DTF (Fig. 5c) has a frequency spectrum that is shaped more closely to the power spectrum of the signal than the normalized DTF (Fig. 5b), for which a more smoothed spectral shape is seen.
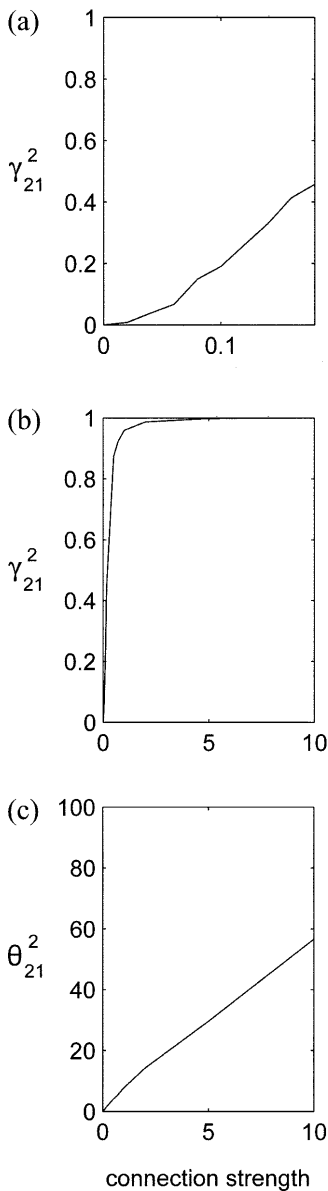
Fig. 4a–c. Dependency of the DTF functions on the coupling strength between the two neural populations. **a** Normalized DTF at low connection strengths; **b** normalized DTF over full range of connection strengths; **c** non-normalized DTF over full range of connection strengths

3.2 Three-channel LFP model

For a mutichannel data set, one can always perform pairwise analysis by fitting AR models for each distinct pair of data channels. In this case the DC measure and the DTF functions give equivalent information. However, performing pairwise evaluation for multichannel data has the drawback that one cannot discern whether the influence between the two channels is direct or is mediated by the other channels. One may even arrive at a wrong conclusion using only a pair of channels that could otherwise be avoided by using the full channel set, as shown below. In this regard, employing the DC measure with the full multivariate data model is an important way
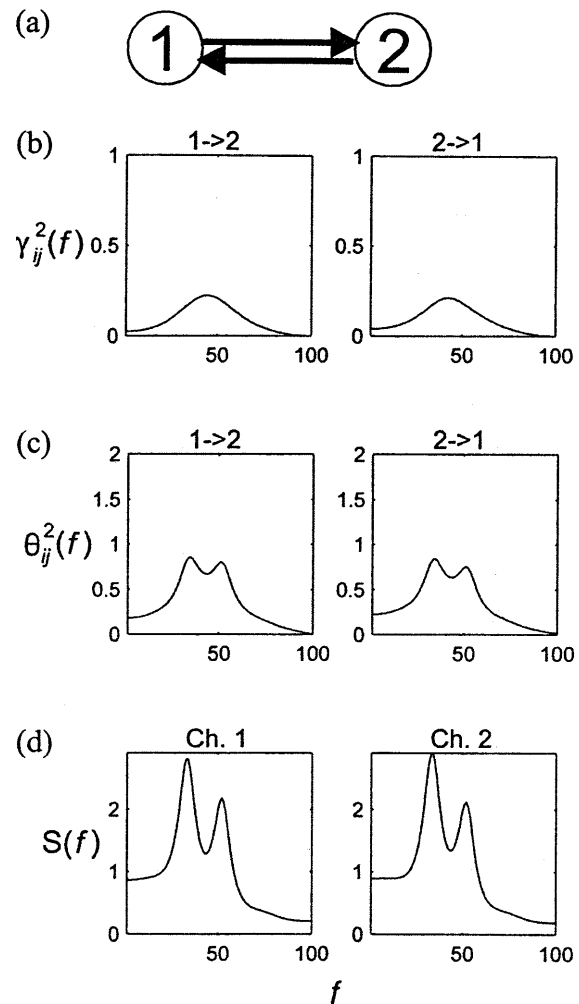

Fig. 5a–d. Results of a two-channel LFP model where the coupling is reciprocal. **a** Coupling scheme; **b** normalized DTF; **c** non-normalized DTF; **d** power spectra; **b**–**d** plotted as functions of frequency (Hz)

to gain further insight into the network connectivity. We illustrate these points with a three-channel LFP model.

We consider two coupling schemes. In the first coupling scheme, as shown in Fig. 6a, channel 3 drives both channel 1 and channel 2, while channel 1 and channel 2 are not coupled. Furthermore, the signals from channel 3 undergo different delays, Δ_1 and Δ_2 respectively, $\Delta_2 > \Delta_1$, before reaching channels 1 and 2. Using only data from channel 1 and channel 2, not knowing the influence of channel 3, one sees a causal influence from channel 1 to 2 due to the difference in the delays. This is shown in Fig. 6b for the non-normalized DTF. When signals from all three channels are fit into a single three-variable MVAR model of order 7, we obtain much better network resolution. Neither normalized (Fig. 6c) nor non-normalized (Fig. 6d) DTF functions show a causal influence between channels 1 and 2, in agreement with the built-in network connectivity pattern. This is because, by including the third channel, the MVAR model properly accounts for the similarity between channel 1 and channel 2 as being due to the common input from channel 3.

As can be seen from (18), the existence of nonzero DTF functions between two channels does not neces-
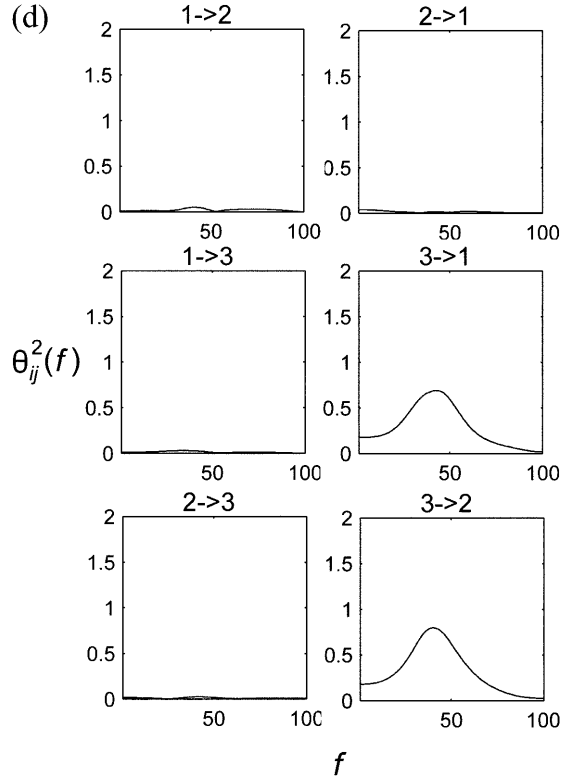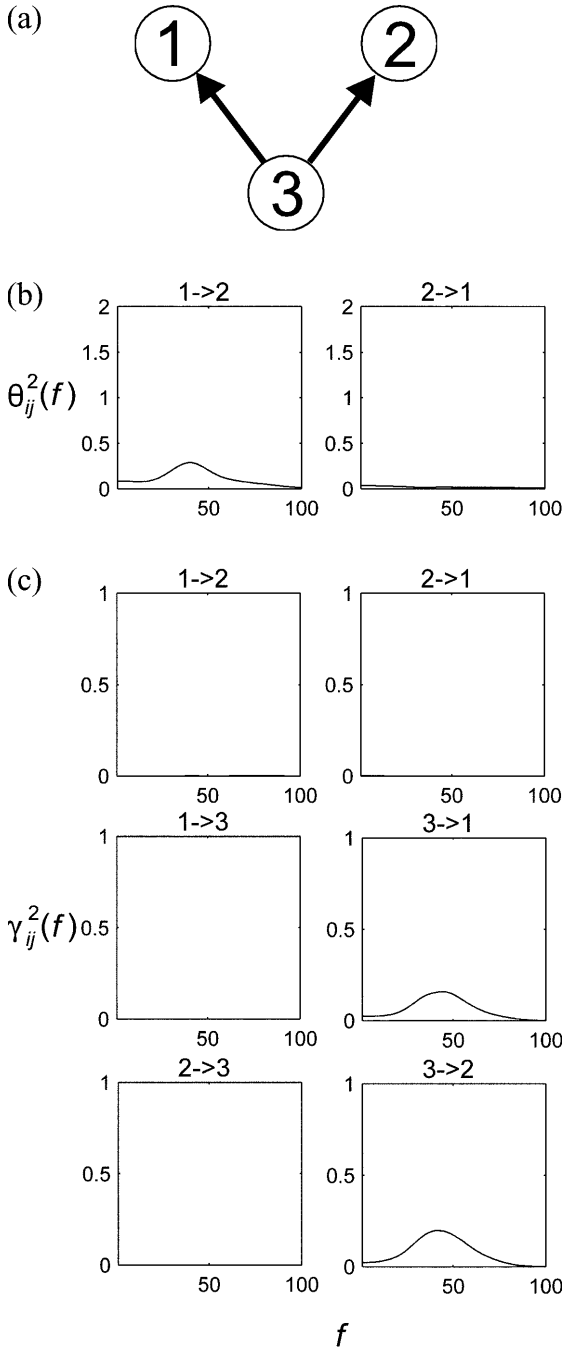
(a)

(b)

$\theta_{ij}^2(f)$

1->2

2->1

(c)

1->2

2->1

$\gamma_{ij}^2(f)$

1->3

3->1

2->3

3->2

f

(d)

$\theta_{ij}^2(f)$

1->2

2->1

1->3

3->1

2->3

3->2

f

Fig. 6a–d. Results of a three-channel LFP model. **a** Coupling scheme; **b** non-normalized DTF where only data from channels 1 and 2 are used in the autoregressive model fitting; **c** normalized DTF; **d** non-normalized DTF where data from all three channels are used in the model fitting

sarily imply a direct linkage between them. In fact, DTF functions represent a linear combination of causal influences along all causal pathways – direct and indirect – originating from one channel and terminating at the other. To examine this question more carefully, we consider the second coupling scheme, shown in Fig. 7a, where we add a connection from channel 1 to channel 3 in addition to the connections in Fig. 6a. This new link opens an indirect causal pathway from channel 1 to channel 2 through channel 3. As expected, both the normalized and non-normalized DTF functions from channel 1 to channel 2 are now nonzero (Fig. 7b, c).

The behavior seen in Fig. 7 raises the question of whether – when an influence from one channel to another is observed with the DTF functions – a direct causal in-

fluence exists between the channels, or whether the influence is entirely due to indirect causal pathways. To address this question, the DC measure discussed in the previous section becomes an important tool. For the coupling scheme in Fig. 7a, the DC measure from channel 1 to channel 2 is $D_{21}^2 = 0.0041$, where no connection exists, as compared to the three real direct connections for which the DC measures are an order of magnitude larger (e.g., $D_{31}^2 = 0.0814$). Thus, because it is only sensitive to direct influence, the DC measure does not show an effect from channel 1 to channel 2, unlike the DTF function which includes indirect influences. Another benefit of the DC measure is that it can also indicate the existence of a causal link between channels, even when the DTF function is zero, as illustrated in Appendix A.
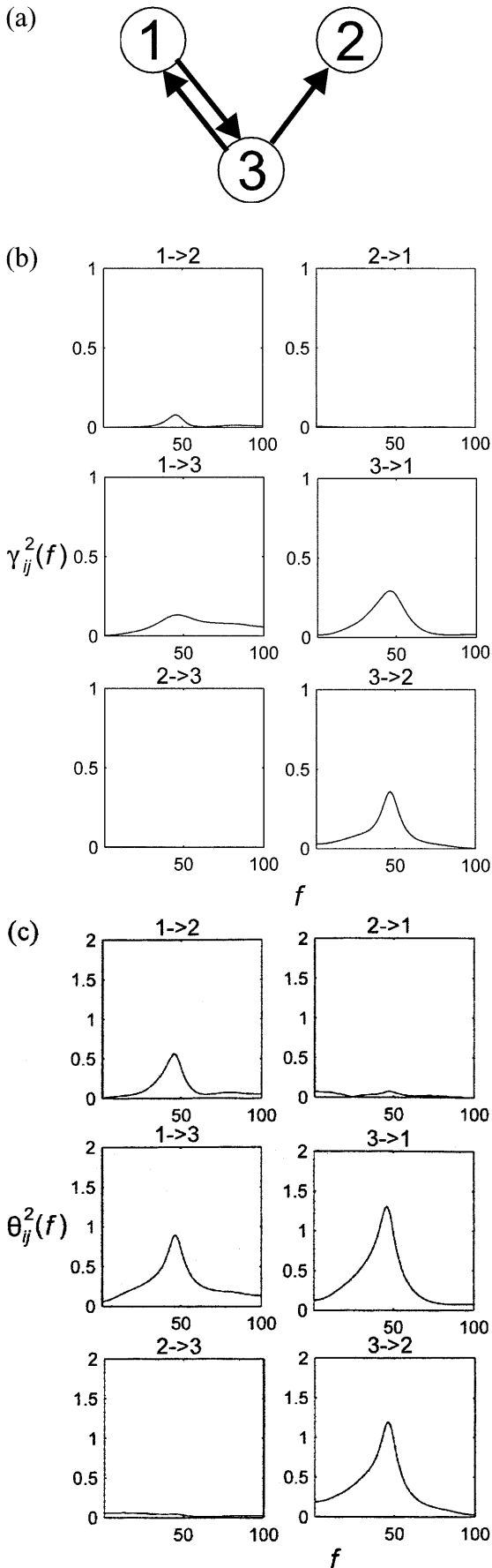
Fig. 7a–c. Results of a three-channel LFP model where the coupling is modified from Fig. 6. **a** Coupling scheme; **b** normalized DTF; **c** non normalized DTF; **b–c** plotted as functions of frequency (Hz)

3.3 Spike train models

Causality analysis is not limited to field-potential data. Here we show that, despite the need for AR model fitting, DTF functions can also be applied to the analysis of multiple spike trains after proper filtering.
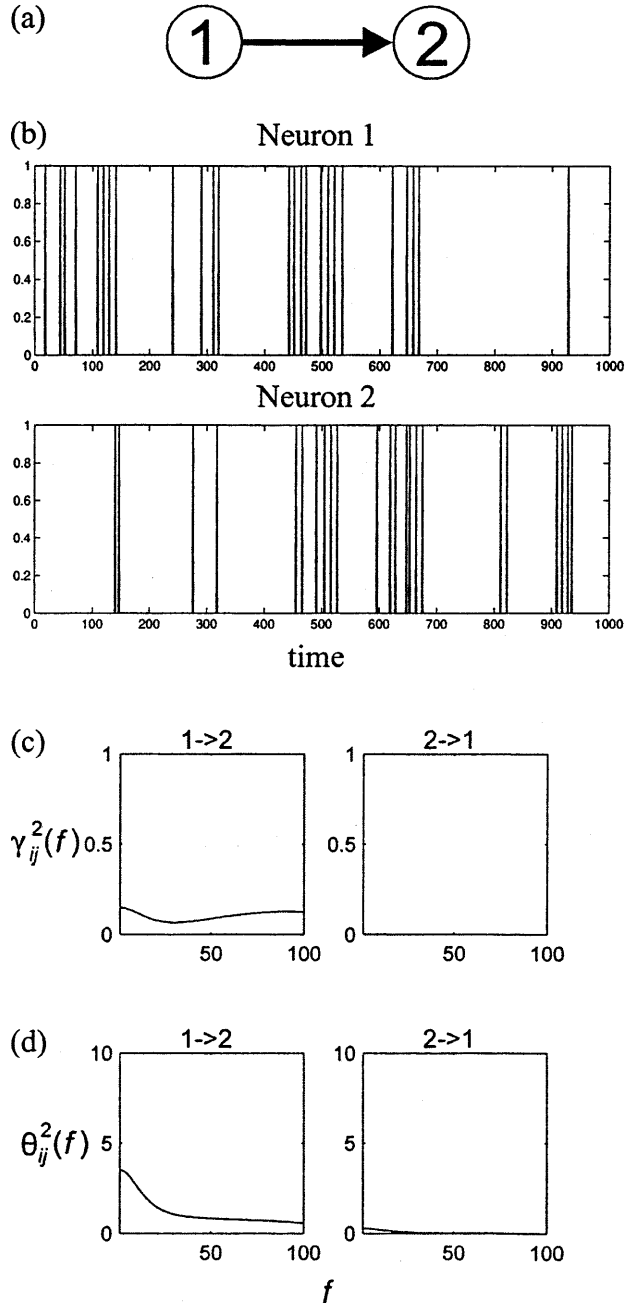

Fig. 8a–d. Results of a spike train model where the coupling is unidirectional. **a** Coupling scheme; **b** spike trains from both neurons (time axis in ms); **c** normalized DTF; **d** non-normalized DTF; **c–d** plotted as functions of frequency (Hz)
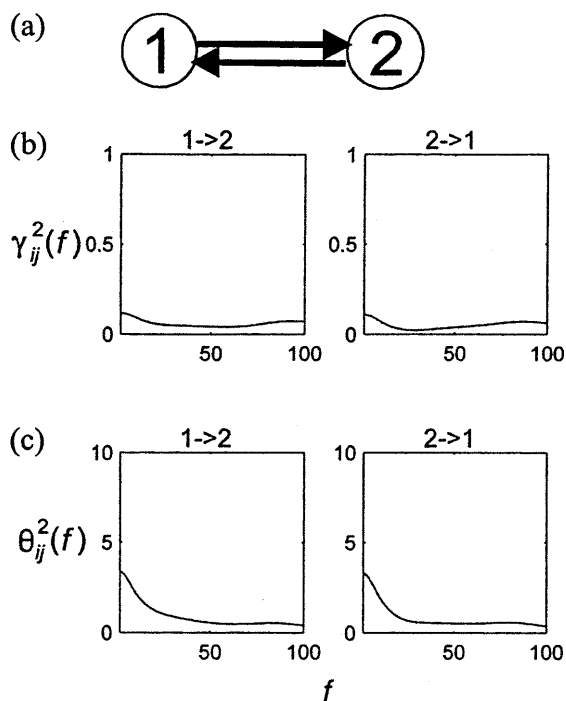
(a)

(b)

(c)

Fig. 9a–c. Results of a spike train model where the coupling is reciprocal. **a** Coupling scheme; **b** normalized DTF; **c** non-normalized DTF; **b–c** plotted as functions of frequency (Hz)

We consider two model neurons in two different connectivity patterns. Mathematical details are given in Appendix C. Figure 8a shows the first coupling scheme, where neuron 1 is unidirectionally coupled to neuron 2. Unfiltered spike trains from both model neurons are shown in Fig. 8b. A data set consisting of 600–1050 spikes from each neuron was analyzed. The spike trains were low-pass filtered (Butterworth filter of order one and cutoff frequency equal to 10% of the Nyquist frequency, filtered in both directions to preserve phase) and a bivariate autoregressive model of order 8 was fit to the filtered data. The normalized and non-normalized DTF functions are shown in Fig. 8c and d. As expected, only the DTF functions from neuron 1 to 2 have significant values, while the functions for the reverse direction are statistically insignificant.

In the second coupling scheme, shown in Fig. 9, the neurons are reciprocally coupled. The DTF functions in Fig. 9b and c show significant influences in both directions, in agreement with the built-in pattern of connectivity.

4 Applications to neurobiological data

4.1 Human sleep analysis

In this example we analyze a data set consisting of a 20-min sample of scalp EEGs recorded during stage 2 sleep by Professor Szelenberger at the EEG Laboratory of Psychiatry, Hospital of Warsaw Medical Academy. The electrodes were placed according to the international 10–20 system (Rechtschaffen and Kales 1968).
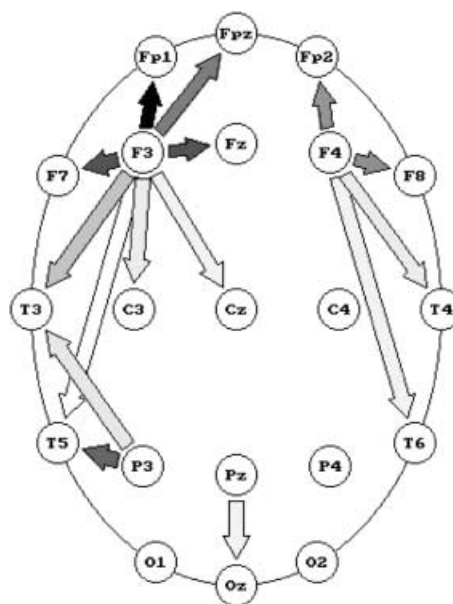

Fig. 10. Patterns of causal influences during stage 2 sleep

The sampling rate was 102.4 Hz. An MVAR model of order 5 was estimated for the 21 channels using the Akaike criterion (Akaike 1974). A more detailed description of the experiment is provided in Kamisńki et al. (1997). Figure 10 shows arrows connecting different recordings channels based on the 15 highest normalized DTF functions, integrated over the 7–15 Hz frequency range. These values are depicted by the gray levels of the arrows.

The DTF pattern in Fig. 10 reveals that the main sources of causal influence are located in the anterior region around the F3 and F4 electrodes, and in the posterior region around the P3 electrode. Influences from these sources are exerted on neighboring and more distant areas within each hemisphere. The paths of causal influence from anterior areas are consistent with prefrontal cortex projection anatomic pathways (Leuchter et al. 1992). In fact, in the transition from wakefulness through stages 1, 2, 3, and 4, we could observe a diminishing role of the posterior sources and an increasing effect of the anterior areas.

Another important issue in this example is the problem of the reference electrode. There are several ways to define a reference electrode in scalp EEG recordings, but not every type is suitable for this analysis. Particularly the "common average" reference which involves all the channels as reference, and mixes signals from all of them, cannot be used. In general, all operations where part of the signal from one channel appears in another channel will lead to spurious connections. In our case the "linked ears" reference was used.

4.2 Analysis of visuomotor integration in macaque monkeys

For sleep studies we often have long and relatively stationary time series available for analysis, and the

application of the MVAR technique is quite straight-forward. During a cognitive task, however, the brain undergoes rapid changes in state, often on a sub-second time scale. These rapid state changes are accompanied by nonstationary time series, requiring that we analyze the data in short windows within which approximate stationarity can be assumed. Studies by Ding et al. (2000) show that by incorporating LFP data from multiple trials performed under the same experimental conditions, one can reliably estimate MVAR models from windows as short as 50 ms. Then, by sliding the analysis window through the entire experimental time course, one obtains a finely resolved picture of cortical dynamics during cognitive processing.

Below, using LFP data recorded from macaque monkeys performing a visuomotor pattern discrimination task, we show that this short window approach combined with causality analysis provides a powerful tool for studying important questions in visual perception. LFP data were recorded by Dr. Richard Nakamura at the National Institutes of Mental Health, Washington, D.C. Transcortical bipolar electrodes were chronically implanted at 15 distributed sites in multiple cortical areas of one hemisphere as the monkey performed a visuo-motor pattern discrimination task (Bressler et al. 1993). The prestimulus stage began when the monkey depressed a hand lever. This was followed 0.5–1.25 s later by the appearance of a visual stimulus (a four-dot pattern) on a computer screen. The monkey made a GO (releasing the lever) or NO-GO (maintaining lever position) response depending on the stimulus category and the session contingency. The entire trial lasted about 500 ms, during which the LFPs were recorded at a sampling rate of 200 Hz. The specific data set considered here consisted of 888 trials from one monkey with the GO response.

For the purpose of data analysis, each of the 15 electrode recording sites was considered to be a separate data channel. As the first step of preprocessing, we detrended the single-trial LFP time series of each channel, subtracted the temporal mean of the entire trial and divided by the temporal standard deviation. The result was that the data from each channel and each trial were given equal weight in model estimation. For the next step of preprocessing, we subtract the ensemble mean from each channel, and normalize the data by dividing by the ensemble standard deviation. The meaning of these steps is explained in Ding et al. (2000). After data preprocessing, a 12-point data window (60 ms) was used for the sliding window analysis, and MVAR models of order 5 were fit to the data from each successive window.

Previous work using power and coherence analysis on the same data set has established the formation of a strong interdependency pattern involving all 15 sites after stimulus presentation, based on highly significant spectral coherence peaks near 12 Hz (Bressler et al. 1999). Since spectral coherence is a symmetric measure, though, it does not provide information on the direction of influence. We calculated the normalized DTF function as a function of time and shown in Fig. 11 the result at the peak frequency of 12 Hz for two channels, one in
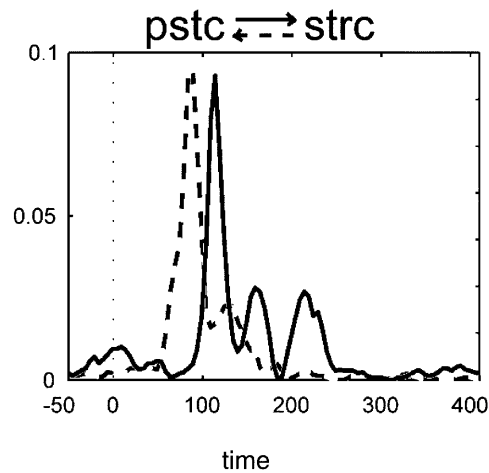

Fig. 11. Normalized DTF functions at 12 Hz plotted as functions of time (ms) using the sliding window technique. The *broken line* represents causal influence from a striate (*strc*) to a prestriate (*pstc*) channel and the *solid line* in the opposite direction. Time zero is the stimulus onset

the striate area and the other in the prestriate area. The broken line represents causal influence from the striate channel to the prestriate channel, and the solid line represents the feedback influence. We see clearly that the stimulus-triggered causal influence from the striate site to the prestriate site begins at about 50 ms poststimulus, while the feedback influence from the prestriate site to the striate site arises at a later time, around 100 ms (here stimulus onset occurs at time zero). Theoretically it is expected that higher visual areas would begin to influence lower areas after first receiving stimulus information from the lower areas. Our result is not only consistent with this theoretical hypothesis, but also provides concrete timing information concerning the onset of feedforward and feedback influences. A more detailed study of causal relations involving more recording sites during visual processing has been presented elsewhere (Liang et al. 2000).

5 Conclusions

In this paper we studied the question of how to evaluate causal relations in neural systems. We showed that the DTF functions and the DC measure are useful and complementary statistical quantities for this purpose that are easy to implement and can be interpreted in the framework of Granger causality. The behavior of these measures was examined both for simulated data and for actual neurophysiological recordings. We emphasized that, for cognitive experiments where the brain changes states on a sub-second time scale, combining causality measures with the short window AMVAR method (Ding et al. 2000) is an important approach for obtaining a finely resolved spatial-temporal picture of cortical dynamics.

Despite their promise, the techniques considered in this paper also have some limitations. First, given that one can only measure from a small number of variables, the interpretation of causal influence is limited to these

measured variables. It is thus crucial that the placement of recording sites be carefully chosen to maximize the power of subsequent causality analysis. Second, although useful in its present form, the DC measure has no frequency dependence. Sameshima and Baccala (1999) introduced a Fourier-transformed version of the DC measure used here, called the partial directed coherence. However, our examination of this quantity indicates that its frequency characteristics are not consistent with that of the signal, making it hard to interpret within the overall frequency structure of the data. Third, our attempt at developing a technique for testing statistical significance remains rudimentary. The surrogate data method destroys both interdependency among time series as well as the temporal structure within a time series. More advanced surrogate data methods, such as those that randomize the sequential order while preserving the correlation structure (Theiler et al. 1992), need to be developed and studied. These questions will be the topics of future investigations.

Appendix A

It suffices to consider a three-channel MVAR model. From (18) it is clear that $H_{21}(f)$ will be zero if

$$A_{21}(f)A_{33}(f) = A_{31}(f)A_{23}(f)$$

Letting $z = e^{-2\pi i f}$ this equation can be rewritten as:

$$\left(-\sum_{j=1}^{p}A_{21}(j)z^{-j}\right)\left(1 - \sum_{j=1}^{p}A_{33}(j)z^{-j}\right)$$
$$= \left(-\sum_{j=1}^{p}A_{31}(j)z^{-j}\right)\left(-\sum_{j=1}^{p}A_{23}(j)z^{-j}\right)$$

For $p = 1$ this leads to:

$$A_{21}(1) = 0$$
$$A_{31}(1)A_{23}(1) = 0$$

meaning that, for a first-order MVAR model, a zero value of DTF implies no direct or indirect causal influence.

For $p = 2$, we obtain a set of conditions:

$$-A_{21}(1) = 0$$
$$-A_{21}(2) = A_{31}(1)A_{23}(1)$$
$$A_{21}(2)A_{33}(1) = A_{31}(1)A_{23}(2) + A_{31}(2)A_{23}(1)$$
$$A_{21}(2)A_{33}(2) = A_{31}(2)A_{23}(2)$$

Consider the simplest case where $A_{33}(1) = A_{33}(2) = A_{23}(2) = A_{31}(2) = 0$ and assume that the second condi-

tion holds. The corresponding time-domain MVAR model equations are:

$$X_1(t) = E_1(t)$$
$$X_2(t) = A_{21}(2)X_1(t-2) + A_{23}(1)X_3(t-1) + E_2(t)$$
$$X_3(t) = A_{31}(1)X_1(t-1) + E_3(t)$$

The equation for $X_2(t)$ can be rewritten as:

$$X_2(t) = A_{21}(2)X_1(t-2) + A_{23}(1)A_{31}(1)X_1(t-2)$$
$$+ A_{23}(1)E_3(t-1) + E_2(t)$$
$$= [A_{21}(2) + A_{23}(1)A_{31}(1)]X_1(t-2) + E_2'(t)$$

We see that when $-A_{21}(2) = A_{31}(1)A_{23}(1)$, the coefficient for $X_1(t-2)$ vanishes. This means that even though we have a direct causal influence from channel 1 to 2 and an indirect influence from channel 1 to 2 through channel 3, they cancel each other, and the overall DTF function from channel 1 to 2 is zero.

Appendix B

Our simulation model is composed of N coupled cortical columns where each column is made up of an excitatory and an inhibitory neuronal population. The equations for the nth column read (Freeman 1992):

$$\frac{d^2x_n}{dt^2} + (a+b)\frac{dx_n}{dt} + abx_n = -k_{ei}Q(y_n(t), Q_m)$$
$$+ \sum_{p}^{N} k_{np}Q(x_p(t+\tau_{np}), Q_m)$$
$$+ \xi_{x_n}(t)$$

$$\frac{d^2y_n}{dt^2} + (a+b)\frac{dy_n}{dt} + aby_n = k_{ie}Q(x_n(t), Q_m) + \xi_{y_n}(t)$$

Here x and y represent LFPs of the excitatory and inhibitory populations, respectively, $k_{ie} > 0$ gives the coupling gain from the excitatory (x) to the inhibitory (y) population, and $k_{ei} > 0$ is the strength of the reciprocal coupling. Neuronal populations are coupled through a sigmoidal function, $Q(x, Q_m)$, representing pulse densities converted from x with Q_m a modulatory parameter:

$$Q(x, Q_m) = \begin{cases} Q_m(1 - e^{-(e^x-1)/Q_m}) & \text{if } x > -u_0 \\ -1 & \text{if } x \le -u_0 \end{cases}$$
$$u_0 = -\ln\left(1 + \ln\left(1 + \frac{1}{Q_m}\right)\right)$$

The coupling strength k_{np} is the gain from the excitatory population of column p to the excitatory population of column n, with $k_{np} = 0$ for $n = p$. The term τ_{np} is the time delay in the transmission. The terms containing $\xi(t)$ represent independent Gaussian white noise inputs given to each neuronal population. The LFPs from all the excitatory populations constitute the multichannel measurement set.

The following parameter values were employed for all the examples presented from Figs. 1–7: $a = 0.22$ /ms, $b = 0.72$ /ms, $k_{ie} = 0.1$, $k_{ei} = 0.4$, $Q_m = 5$, and the noise was zero mean with variance $\sigma_\xi^2 = 0.04$. The time delays were all set to $\tau = 15$ ms unless mentioned otherwise. The coupling strengths between columns used for different examples are as follows. For Figs. 1–3: $k_{12} = 0$ and $k_{21} = 0.1$; for Fig. 4: the coupling strengths used are $k_{12} = 0$ and $k_{21} = 0, 0.02, 0.04, 0.06, 0.08, 0.1, 0.12, 0.14, 0.16, 0.18, 0.5, 0.7, 1, 2, 5, 10$; for Fig. 5: $k_{12} = k_{21} = 0.1$; for Fig. 6: $k_{13} = k_{23} = 0.6$ are the nonzero couplings, $\tau_{13} = 15$ ms, $\tau_{23} = 25$ ms; and for Fig. 7: $k_{13} = k_{23} = k_{31} = 0.1$, $\tau_{13} = 15$ ms, $\tau_{23} = 25$ ms, and $\tau_{31} = 10$ ms.

The equations were integrated using the following procedure. At each integration step: (A) the deterministic part of the equations were solved by using a fourth-order Runge-Kutta method with linear interpolation for the delays; (B) the noise term was integrated using the Euler method; and (C) the results from (A) and (B) were added to give the final value. The integration step size was 0.1 ms. We sampled the data at 200 Hz. All simulations were implemented in the C programming language on a PC computer.

Appendix C

Excitatory neurons were modeled as single-compartment integrate-and-fire neurons using known cellular parameters (Lumer et al. 1997). The instantaneous change of the membrane potential V_i of each neuron model i was given by:

$$\tau_m \frac{dV_i(t)}{dt} = -V_i + E_0 - g(t)(V_i - E)$$

where τ_m is the membrane time constant and E_0 is the resting membrane potential. When V_i reached the spike threshold a spike was recorded and the membrane potential was reset. The spike was relayed to the target synapses with a transmission delay of 5 ms. The synapses were modeled as AMPA conductance changes $g(t)$ according to a dual exponential response with characteristic rise and decay times. The term E corresponded to the reversal potential of the channel. All the synapses had the same conductance peak. The refractory period was set to 5 ms. Each neuron had a spontaneous activity obtained with additive lowpass Gaussian noise waveforms independent for each neuron. The equations were integrated using the Euler method with an integration step of 1 ms.

References

Akaike H (1974) A new look at statistical model identification. IEEE Trans Autom Control 19: 716–723

Asher HB (1983) Causal modelling. Sage Publications, Newbury Park, Calif

Bernasconi C, König P (1999) On the directionality of cortical interactions studied by structural analysis of electrophysiological recordings. Biol Cybern 81: 199–210

Bressler SL, Coppola R, Nakamura R (1993) Episodic multiregional cortical coherence at multiple frequencies during visual task performance. Nature 366: 153–156

Bressler SL, Ding M, Yang W (1999) Investigation of cooperative cortical dynamics by multivariate autoregressive modeling of event-related local field potentials. Neurocomputing 26–27: 625–631

Caines PE, Chan CW (1975) Feedback between stationary stochastic processes. IEEE Trans Autom Control 20: 498–508

Ding M, Bressler SL, Yang W, Liang H (2000) Short-window spectral analysis of cortical event related potentials by adaptive multivariate autoregressive modeling: data preprocessing, model validation, and variability assessment. Biol Cybern 83: 35–45

Freeman WJ (1992) Tutorial in neurobiology: from single neurons to brain chaos. Int J Bifurc Chaos 2: 451–482

Gevers MR, Anderson BDO (1981) Representations of jointly stationary stochastic feedback processes. Int J Control 33: 777–809

Geweke J (1982) Measurement of linear dependence and feedback between multiple time series. J Am Stat Assoc 77: 304–324

Granger CWJ (1969) Investigating casual relations by econometric models and cross-spectral methods. Econometrica 37: 424–438

Kamiński MJ, Blinowska KJ (1991) A new method of the description of the information flow in the brain structures. Biol Cybern 65: 203–210

Kamiński M, Blinowska K, Szelenberger W (1997) Topographic analysis of coherence and propagation of EEG activity during sleep and wakefulness. Electroencephalogr Clin Neurophysiol 102: 216–227

Kirk RE (1995) Experimental design. Procedures for the behavioral sciences. Brooks/Cole, Pacific Grove, Calif

Leuchter AF, Newton TF, Cook IA, Walter DO, Rosenberg-Thompson S, Lachenbruch PA (1992) Changes in brain functional connectivity in Alzheimer-type and multi-infarct dementia. Brain 115: 1543–1561

Liang H, Ding M, Nakamura R, Bressler SL (2000) Causal influences in primate cerebral cortex during visual pattern discrimination. Neuroreport 11: 2875–2880

Lumer ED, Edelman GM, Tononi G (1997) Neural dynamics in a model of the thalamocortical system. I. Layers, loops and the emergence of fast synchronous rhythms. Cereb Cortex 7: 207–227

Rechtschaffen A, Kales A (1968) A manual: standarized terminology, techniques and scoring system for sleep stages of human subjects. Brain Information Service/Brain Research Institute, University of California, Los Angeles

Saito Y, Harashima H (1981) Tracking of information within multichannel EEG record. In: Yamaguchi N, Fujisawa K (eds) Recent advances in EEG and EMG data processing. Elsevier, Amsterdam, pp 133–146

Sameshima K, Baccalá LA (1999) Using partial directed coherence to describe neuronal ensemble interactions. J Neurosci Methods 94: 93–103

Schack B, Grieszbach G, Arnold M, Bolten J (1995) Dynamic cross-spectral analysis of biological signals by means of bivariate ARMA process with time-dependent coefficients. Med Biol Eng Comput 33: 605–610

Schnider SM, Kwong RH, Lenz FA, Kwan HC (1989) Detection of feedback in the central nervous system using system identification techniques. Biol Cybern 60: 203–212

Theiler J, Eubank S, Longtin A, Galdrikian B, Farmer JD (1992) Testing for nonlinearity in time series: the method of surrogate data. Physica D 58: 77–94

Wang G, Takigawa M (1992) Directed coherence as a measure of interhemispheric correlation of EEG. Int J Psychophysiol 13: 119–128

Wiener N (1956) The theory of prediction. In: Beckenbach EF (ed) Modern mathematics for engineers, chap 8. McGraw-Hill, New York